JOURNAL OF AIRCRAFT
Vol. 31, No. 6, November–December 1994

Effect of Underwing Frost on a Transport Aircraft Airfoil at Flight Reynolds Number

M. B. Bragg* and D. C. Heinrich†
University of Illinois at Urbana–Champaign, Urbana, Illinois 61801
W. O. Valarezo‡
McDonnell Douglas Aerospace, Long Beach, California 90846
and
R. J. McGhee§
NASA Langley Research Center, Hampton, Virginia 23681

The effect of underwing frost on a transport aircraft airfoil in a takeoff configuration was studied. Underwing frost can occur when the lower surface of the wing is cooled by fuel cold-soaked in the wing tanks during cruise. Frost may accrete on the wing lower surface while the aircraft is awaiting takeoff. A two-dimensional test was performed in the NASA Langley Low-Turbulence Pressure Tunnel on a representative high-lift airfoil with a leading-edge slat and trailing-edge flap. Frost was simulated on the lower surface using distributed roughness particles. The test was conducted at $M = 0.2$ and $Re = 5 \times 10^6$ to 1.6×10^7. The effects of the frost on performance were generally small, with the largest effects occurring for the open-slat case with the frost starting at 12% chord. In this situation, it was found that the frost contaminated the upper surface boundary layer at high angles of attack, increasing drag and reducing maximum lift.

Nomenclature

C_d = airfoil drag coefficient, drag/qc
C_l = airfoil lift coefficient, lift/qc
c = airfoil chord length
k = roughness height
q = air dynamic pressure, $\frac{1}{2}$(air density)V^2
Re = Reynolds number, Vc/ν
t = frost thickness
V = tunnel velocity
x = airfoil chordwise position
α = airfoil angle of attack
Δ = frost/ice value minus the chosen baseline value
ν = kinematic viscosity of the air

Subscripts
frost = frost case
max = maximum value
s, stall = airfoil stall
0 = minimum value
1 = critical engine failure
2 = takeoff climb

Introduction

TRANSPORT aircraft usually cruise for extended periods of time at high altitude where the ambient temperature is well below freezing. Under these conditions the fuel in the wing tanks will reach low temperatures. The fuel in this case is often referred to as "cold-soaked." After landing, the remaining fuel in the wing tanks can cool the wing lower surface to temperatures below freezing. The wing area affected is very dependent upon the wing tank location, the amount of fuel remaining, the fuel temperature, and the design of the wing structure and the tanks.

If the ground level humidity is high, moisture in the air will condense on the aircraft wings in the location of the cold fuel to form frost. Ice may form if the frost partially melts, the resulting water then flows toward the fuselage due to the wing dihedral, and refreezes. The frost usually occurs on the undersurface of the wing, usually confined by the front and rear spar locations, and is thus termed "in-spar" frost.

Many researchers have studied the effect of roughness on airfoils, wings, and aircraft performance. Ljungstroem[1] studied experimentally the effect of upper surface frost on two-dimensional airfoil performance. These airfoils had high-lift devices, but only upper surface and leading-edge frost was investigated. Bragg and Gregorek[2] considered the effect of roughness from several different sources on laminar flow airfoils. While this study did include some consideration of overall aircraft performance, again only leading-edge roughness was considered. A correlation of roughness effects on maximum lift was presented by Brumby.[3] This study also considered only upper-surface and leading-edge roughness. Valarezo et al.[4] conducted experimental measurements on a multielement airfoil with a leading-edge device and roughness in the NASA Langley Low-Turbulence Pressure Tunnel. Testing over a range of Reynolds numbers from 2.5×10^6 to 1.8×10^7, they noted difficulty in applying low Reynolds number data to high Reynolds number applications. Valarezo[5] carried out high Reynolds number investigations on the performance effects of ground frost (upper surface) simulations. These studies, and many more not discussed here, all have investigated the effect of leading-edge or upper-surface frost or roughness. Results on lower-surface frost effects at high Reynolds number have not been available.

Computational and empirically based studies of frost and roughness effects have been performed with upper-surface and leading-edge roughness. Bragg and Gregorek,[6] and later Kind and Lawrysyn,[7] developed two-dimensional computational methods to predict roughness effects on single-com-

Received Nov. 2, 1993; revision received March 6, 1994; accepted for publication March 15, 1994.

*Associate Professor, Department of Aeronautical and Astronautical Engineering. Associate Fellow AIAA.
†Graduate Research Assistant, Department of Aeronautical and Astronautical Engineering. Member AIAA.
‡Principal Engineer, Aerodynamics Technology, Boeing Commercial Airplane Group. Senior Member AIAA.
§Head, Low-Turbulence Pressure Tunnel Section, Experimental Flow Physics Branch. Member AIAA.

Table 1 Simulation of underwing frost

Frost/ice simulation	k/c[b]	Roughness extent, x/c	Full scale		Model[a]	
			k, in.	Concentration/in.^{2}	k, in.	Concentration/in.^{2}
Typical frost	0.00011	0.16–0.60	0.016	30	0.0029–0.0035	852
Typical frost	0.00011	0.20–0.60	0.016	30	0.0029–0.0035	852
Large frost/ice	0.00040	0.12–0.60	0.059	12	0.0083–0.0098	480
Large frost/ice	0.00040	0.20–0.60	0.059	12	0.0083–0.0098	480
Large ice	0.00085	0.12–0.60	0.125	10	0.0165–0.0197	135

[a]Actual values determined from grit number information and measured roughness element concentrations. [b]Assumes c = 12.21 ft.

ponent airfoils. Kind and Lawrysyn also report some detailed work on classifying frost by its effect on the turbulent boundary layer. Studies on the effect of frost or roughness on the takeoff performance of aircraft have been reported by Dietenberger[8] and van Hengst and Boer.[9] Both of these reports use empirical methods based on experimental data as input to computational takeoff analyses. Therefore, the takeoff analysis methods have been developed, but what is missing is the experimental data on lower-surface roughness or frost effects on representative airfoils.

Brumby[10] and Langston[11] report that typical frost grains are from 0.003 in. in height to large frail needles 0.015 in. in height. Thompson[12] and Langston[11] both discuss the large needles and their tendency to be blown off during the takeoff run at speeds from 20 to 40 mph.[12] Thompson also presents data on the weight of frost accretions on wings. "Spiky" frost needles[12] can have sizes up to $\frac{1}{8}$ or even $\frac{1}{4}$ in. A later study conducted by Kind and Lawrysyn[13] revealed that frost samples as high as 1 mm (0.039 in.) could be grown on flat plates. Kind's study is the most extensive frost study conducted in the last few years, and a frost height of 0.4 mm was chosen as a typical value.

Langston[11] and Brumby[10] both discuss the phenomenon of the frost as it grows, building upon itself in layers. This leads to the difference between the thickness of the frost and the aerodynamic roughness height. This distinction is important for the very thick frost sometimes reported in the literature. While the overall thickness may cause small changes in the wing contour, it is the aerodynamic roughness that causes the aerodynamic penalties. In the work performed here, it is the aerodynamic roughness height that was simulated. To further improve the frost simulation, it is also necessary to model the frost density. According to Kind and Lawrysyn's study,[7] the full-scale densities for the heights considered here range from 12 to 30 particles/in.^{2}. In determining a density, only the highest 20% of the frost grains were counted.

In this study, the available information on the characteristics of frost were used to simulate frost formations on an airfoil lower surface. Two-dimensional wind-tunnel tests were conducted at flight Reynolds numbers to measure the effect of simulated underwing frost on transport airfoil takeoff performance. These data are then available for application to aircraft takeoff performance calculations for aircraft with underwing frost.

Experimental Method

The airfoil test was conducted in the NASA Langley Low-Turbulence Pressure Tunnel with simulated frost at near-takeoff Reynolds numbers for a transport aircraft. While three-dimensional tests would be desirable, only low Reynolds number facilities were available that would have required extensive roughness scaling. This section briefly describes the tunnel, airfoil model, roughness modeling, and data acquisition.

Tunnel and Model Description

A supercritical high-lift transport airfoil[14] was tested at the Low-Turbulence Pressure Tunnel (LTPT) at NASA Langley. The LTPT is a single-return closed throat wind tunnel with a 3-ft-wide, 7.5-ft-long and 7.5-ft-high test section. It is capable

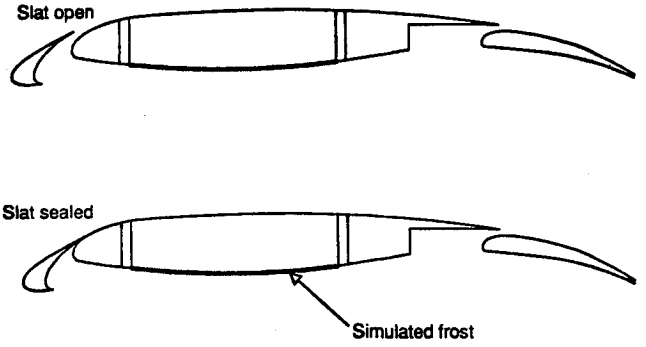

Fig. 1 Transport airfoil model in takeoff configuration.

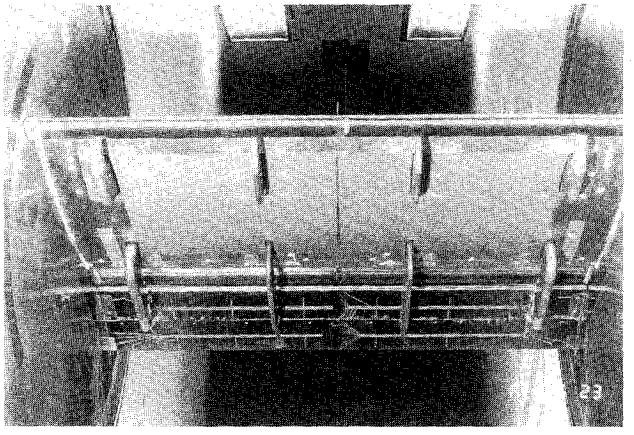

Fig. 2 Model in the tunnel with underwing frost simulation installed on the lower surface from 12 to 60% chord.

of running at pressures up to 10 atm to increase the density, and consequently, allow tests at flight Reynolds numbers at low subsonic Mach numbers typical of takeoff and climb. Boundary-layer suction was used on the sidewalls to promote two dimensionality of the multielement model flowfield.[15]

The airfoil model used in this study was representative of current supercritical airfoil technology for transport aircraft. Specifically, the airfoil consisted of a leading-edge slat, a main element, and a single element flap. The cross section is shown in Fig. 1. The airfoil had a chord of 22 in. and spanned the 3-ft-wide tunnel test section. The slat was 0.1448c and the flap chord was 0.3c. Figure 2 shows a photograph of the model in the tunnel. The airfoil was tested with the slat deflected 20 deg and the flap deflected 15.6 deg at representative gaps and overhangs. The model surface pressure could be sensed from the 142 pressure taps distributed chordwise on the model centerline. The airfoil was tested with the slat open and closed to model airfoil takeoff configurations currently in use.

Frost Simulation and Boundary-Layer Trips

Table 1 summarizes the full-scale frost/ice values simulated and the actual roughness values tested on the model. The typical frost simulation has a full-scale roughness size of 0.016 in. and is similar to that used by Kind and Lawrysyn.[7] The large frost/ice simulation provides an upper bound on frost

grain roughness and a simulation of ice beads. The large ice simulation represents a worst case for the frost that melts and refreezes as water droplets. Large ice is assumed to be $\frac{1}{8}$-in. full scale, larger than is usually seen in practice, but is included as an upper bound on the frost/ice roughness problem.

The frost or ice simulations used extended from the 12 to 60, or 20 to 60% chord location on the lower surface of the airfoil. The 12 and 20% chord values for the leading edge of the frost coverage were chosen because they correspond approximately to the range of values for the leading edge of the main fuel tanks in current transport aircraft. The 60% chord location is representative of the most rearward extent of the fuel tanks on current transport aircraft. To save application time, no roughness was applied between the outboard flap support bracket and the tunnel wall on each side (Fig. 2). This was appropriate since all aerodynamic data were acquired on the model centerline.

Applying the roughness, particularly the very small grit, is very difficult. Sandpaper was considered as a possibility for modeling the frost as Ljungstrom[1] had done. However, sandpaper has a backing that is too large, and thus would appear as a two-dimensional step. Applying sand grain roughness directly to the model surface with adhesive was also considered, but according to Kind and Lawrysyn,[7] the ratio of sand grain height to frost height varies widely. Also, if sand grain roughness was to be used, the amount of grit to be applied would be excessive for the present simulations. Consequently, considering the problems involved with the sand grain roughness and the range of model frost heights necessary, Ballotini beads applied with adhesive at the scaled density was the technique selected.

The roughness elements were sprayed onto the lower surface using a specially designed air pressure sprayer. A 0.005-in.-thick application of red, fast-drying paint was used as an adhesive and to provide a high-contrast background for photography. A clear plastic grid of 0.01-in. squares was placed over the roughness application and photographed using a 35mm camera with a macro lens. The roughened surface was photographed at 20 locations on the model and the data averaged to get the reported roughness density (Table 1).

The boundary-layer development on a swept wing can be quite different than that on a two-dimensional airfoil section, even if Reynolds number and Mach number are held constant. The swept wing boundary layer will transition at the attachment line at higher Reynolds numbers.[16,17] Relaminarization of the flow can occur downstream of a turbulent attachment line in a sufficiently strong favorable pressure gradient.[17] Due to the wing sweep and mild pressure gradients on the wing lower surface, the airfoil lower surface boundary layer should be turbulent from the attachment line. Recent surface hot-film measurements on the lower surface of a similar model tested at NASA Langley has found extensive laminar flow on the lower surface of a two-dimensional model.[18] Figure 3[18] summarizes results obtained using surface hot-film techniques on this same airfoil configured with a 20-deg slat and a 10-deg flap at a chord Reynolds number of 9×10^6. The information is plotted as x/c unwrapped about each element leading edge and as a function of angle of attack. It can be clearly seen that the main element lower-surface boundary layer is essentially laminar over much of the positive α range. It is also interesting to note the substantial laminar/transitional flow and laminar separation bubbles on the flap at this Reynolds number. Therefore, for proper aerodynamic simulation, boundary-layer transition on the lower surface had to be simulated.

The boundary-layer trip strip height was evaluated using the method outlined by Braslow and Knox.[19] The trip was formed by applying a strip of the red paint adhesive $\frac{1}{8}$ in. wide in the chordwise direction. The appropriate grit size was then applied at the desired density. The first trip was located at $x/c = 0.12$ on the lower surface, and had a grit height of 0.006 in., and a density of 1445 particles/in.^{2}. The second trip was located at $x/c = 0.20$ on the lower surface, and had a grit height of 0.006 in., and a density of 363 particles/in.^{2}.

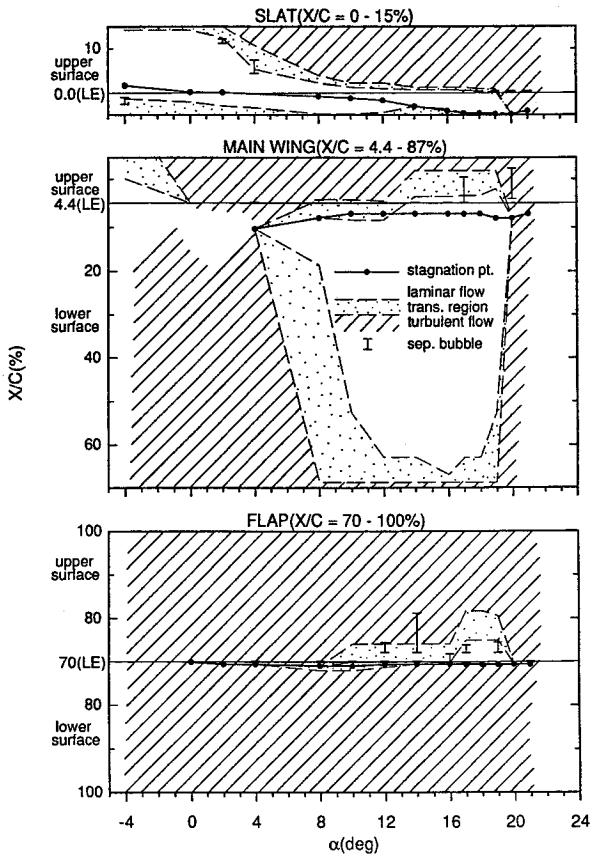

Fig. 3 Boundary-layer state from surface hot-film technique[18] for 20-deg slat and 10-deg flap at $Re = 9 \times 10^6$.

Description of Data and Errors

Using the test setup described, data were taken at angles of attack ranging from 0 to 20 deg. At each angle of attack, the tunnel conditions, surface pressure data, and wake rake data were acquired with an electronically scanned pressure system. The pressure distributions were integrated to obtain airfoil lift and pitching moment coefficients. The model lift coefficient was also available from the facility sidewall balance system. Balance lift coefficient compared well with the pressure data, therefore, only pressure derived lift data are presented here. The drag coefficient data were obtained from a wake survey probe downstream of the model and on the model centerline. Data at 9-, 10-, and 11-deg angle of attack were taken twice and averaged to improve the data quality in this important range as explained below. All of the coefficient data were corrected for tunnel wall and blockage effects using the method outlined in Rae and Pope.[20]

It was anticipated that the lift and drag increments might be small and, therefore, some estimate of the change in airfoil lift and drag to cause a given level of aircraft takeoff performance degradation was desired. The worst case would be the effect of underwing frost on a twin-engine aircraft that lost an engine on takeoff at V_1, the critical decision speed. The critical case for drag is the requirement to maintain level flight in first segment climb, before the landing gear is retracted. The weight can be reduced to return an aircraft with increased drag to the original climb performance by reducing induced drag. Assuming a 100 lb decrease in weight to be significant, a typical twin-engine jet transport would need a 0.0003 increase in parasite drag coefficient over an assumed 50% of wing planform affected by underwing frost. This is then considered the drag significance level, and it occurs at a climb speed of V_2, or a section C_l of approximately 70–80% $C_{l_{max}}$. A significance level of a change in V_{stall} of 1 kt was used to

determine $\Delta C_{l_{max}}$. For the same twin-jet aircraft with 50% of the wing area affected by underwing frost, this yields a significance level of $\Delta C_{l_{max}} = 0.03$. Therefore, in the two-dimensional airfoil data, a change in drag in the range of V_2 of 0.0003 (3 drag counts) and a change in $C_{l_{max}}$ of 0.03 was considered significant in terms of the aircraft takeoff performance.

Repeatability tests were performed by taking multiple measurements while fixed at a given test condition, and for a few configurations by repeating an entire angle-of-attack sweep, a test run. Repeating entire runs showed that the maximum lift coefficient was repeatable to within ± 0.03, and repeating specific data points showed that the sectional drag coefficient was repeatable to within ± 2 drag counts (0.0002). While these values are small, the uncertainty in the data was only equal to or slightly less than the calculated significance levels. This demonstrated that the repeatability was just sufficient to resolve changes in the airfoil performance of importance to the takeoff problem.

Results and Discussion

The results from this study are organized in three sections. First, the data for the model without the lower surface roughness frost simulation is presented. This includes the effect of Reynolds number, slat setting, and boundary-layer trip. The model without frost simulation is referred to as the clean model. The next two sections present the airfoil data with the frost simulation. Since the effects were quite different with and without the slat gap open, the slat gap closed data are presented followed by the slat gap open data.

Clean Model

The clean model was tested at chord Reynolds numbers of 5, 9, 12, and 16 $\times$ 10^6. Figure 4 shows the lift performance of the clean model with the slat gap closed at the 4 different Reynolds numbers at angles of attack from 0 to 19 deg. The data at 9 $\times$ 10^6 and above are almost identical with the 5 $\times$ 10^6 data having a slightly reduced $C_{l_{max}}$. The drag coefficient data for the 4 Reynolds numbers are shown in Fig. 5. The Reynolds number effects on this takeoff geometry are more apparent on drag than lift as discussed in Ref. 21. The drag coefficient increases with decreasing Reynolds number as expected. For example, the drag coefficient at a C_l of 2.1 increases from 0.0165 to 0.0183 as the Reynolds number decreases from 1.6 $\times$ 10^7 to 5 $\times$ 10^6. Note that in both Figs. 4 and 5 the data are more dense between $\alpha = 8$ and 12 deg, and the data at 9, 10, and 11 deg show repeat points. This was done to bracket the range for V_2 for a typical transport aircraft and to improve confidence in data taken over this important region of aircraft takeoff climb.

Figure 6 shows the drag polars for the clean airfoil at Reynolds number 9 $\times$ 10^6 with the slat gap open and closed. At lift coefficients below approximately 2.2, the slat-closed case has a lower drag coefficient, with the opposite being true at

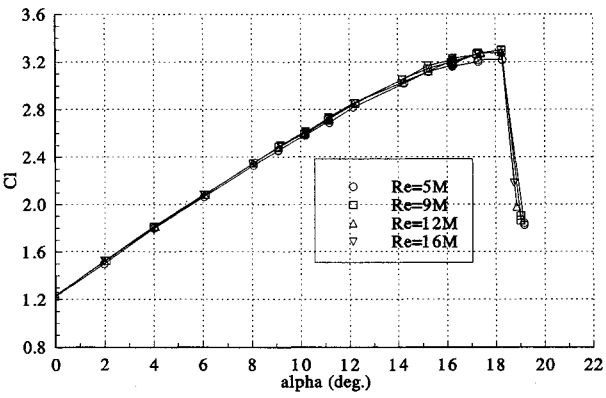

Fig. 4 Effect of Reynolds number on the lift of the clean model, slat-closed.

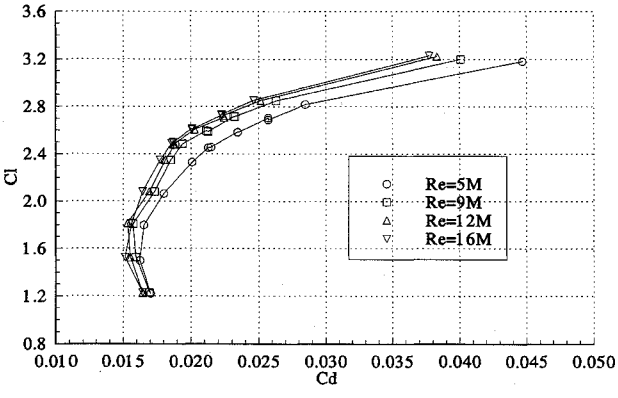

Fig. 5 Effect of Reynolds number on the drag of the clean model, slat-closed.

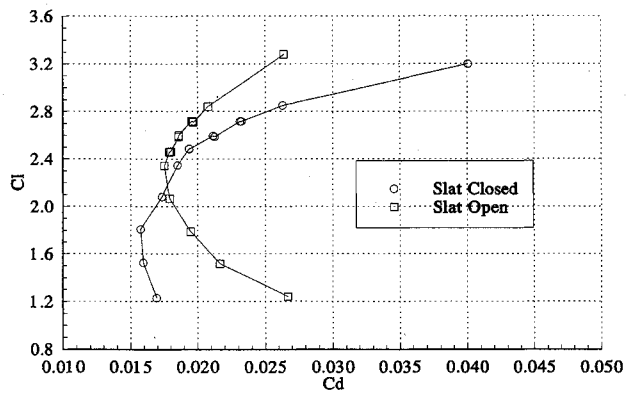

Fig. 6 Drag polars for the slat-open and closed case at Re = 9 $\times$ 10^6.

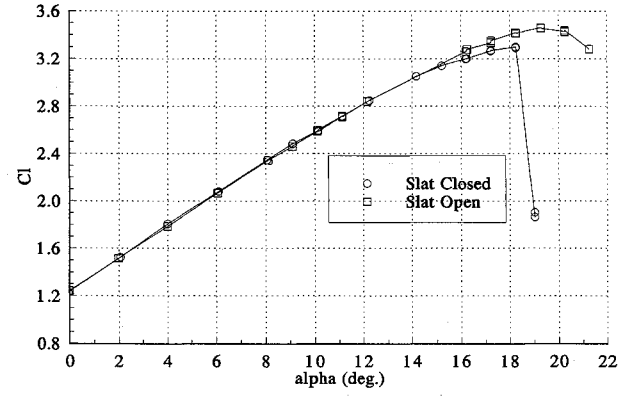

Fig. 7 Lift performance for the slat-open and closed case at Re = 9 $\times$ 10^6.

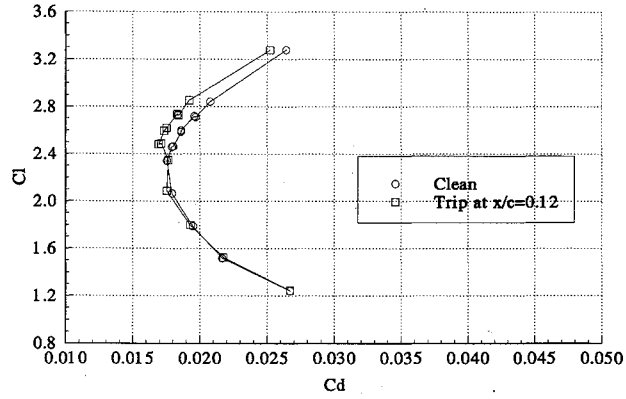

Fig. 8 Drag polars for the clean and tripped case at Re = 9 $\times$ 10^6, slat-open.

lift coefficients above 2.2. Most current transport aircraft takeoff with the slat gap closed to take advantage of the lower drag at lift coefficients seen during takeoff and climb. However, some transports do takeoff slat-open, and so the effect of lower surface frost on both configurations was tested. The lift coefficient data (Fig. 7) show similar performance for the slat-open and closed configurations, except at angles of attack just prior to stall. The slat-closed case stalls sharply at an angle of attack and lift coefficient less than the slat-open case. For this airfoil with the slat at 20 deg and the flap at 15.6 deg, the slat-open configuration stalls at approximately 19 deg angle of attack with a $C_{l_{max}} = 3.46$. The closed configuration stalls one deg earlier with a $C_{l_{max}} = 3.30$.

The most interesting feature of the study is apparent from Fig. 8. Note that at angles of attack above 8 deg, or C_l above 2.3, the presence of the trip actually reduces the drag coefficient by approximately 12 drag counts ($\Delta C_d = 0.0012$). The most logical explanation for this behavior is the presence of a laminar separation bubble on the upper surface, leading edge of the airfoil main element. Surface hot-film results obtained on this same airfoil,[18] but with a 10-deg flap deflection, are shown in Fig. 3. Here, at low angles of attack transitional flow, and at higher angles, a laminar separation bubble was measured on the main element leading edge. The present effect is seen at α above 8 deg, because the stagnation point moves downstream of the lower surface trip location for these angles (with a 15-deg flap deflection). The "lower" surface trip causes early transition to occur in the upper-surface boundary layer, thus eliminating the large transitional region or laminar bubble and reducing the drag coefficient. No clear evidence of a laminar bubble could be found in the surface pressure distributions, although this is not unusual for small bubbles. The boundary-layer trip at $x/c = 0.12$ had almost no effect on the lift coefficient or $C_{l_{max}}$.

While the exact mechanism is unclear, the trip at $x/c = 0.12$ affected the upper surface boundary layer reducing the drag. The available evidence seems to point to a laminar bubble, and this will be assumed in the discussions to follow. Due to the presence of the laminar separation bubble, and its significant effect on the airfoil drag, the presence of the bubble had to be considered in the airfoil tests with simulated lower-surface frost.

Slat-Closed with Simulated Frost

Results of the effect of lower surface frost simulations on the airfoil tested at Reynolds number 9×10^6 are shown in Figs. 9 and 10. The baseline used for this comparison is the clean airfoil with the boundary-layer trip at $x/c = 0.12$ on the lower surface. The lift curve slope was unaffected by the presence of the frost, but the maximum lift coefficient and stall angle were affected. The corresponding drag data are shown in Fig. 10. Here, a trend is more definitive and it can be seen that the drag increased from the baseline as the roughness simulation became more severe. The large ice simulation

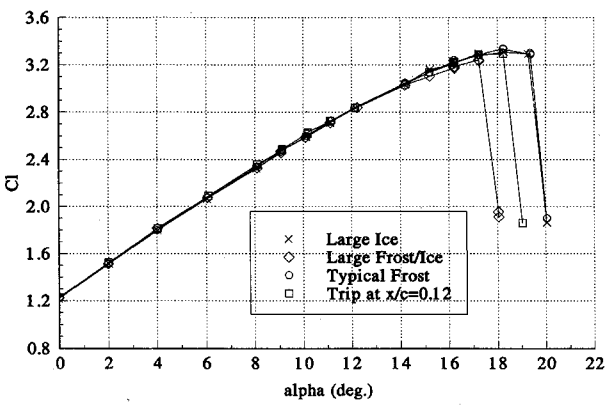

Fig. 9 Effect of simulated frost on lift at $Re = 9 \times 10^6$, slat-closed, and roughness starting at $x/c = 0.12$.

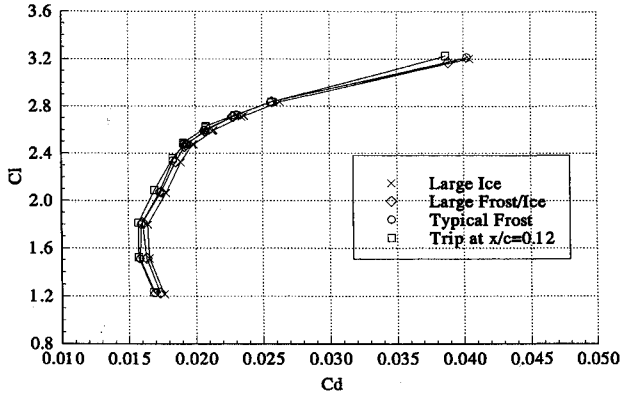

Fig. 10 Effect of simulated frost on drag at $Re = 9 \times 10^6$, slat-closed, and roughness starting at $x/c = 0.12$.

produces a drag increase of approximately 10 counts in the range of V_2.

The effect of the frost and ice simulations on drag and maximum lift are tabulated in Table 2 for the slat-closed case. For both the lift and drag increment the Δ refers to the frost value minus the baseline value. The drag increment of interest is that which occurs near V_2 during the critical first segment climb. It is assumed here that the weight of the frost is small, and that the aircraft will operate at the same airspeeds during takeoff with or without the frost. Therefore, the drag comparison is made at constant lift coefficient. For a typical twin-jet transport, a two-dimensional value of C_l at V_2 between 2.55–2.65 was assumed. The ΔC_d values shown in the tables have been averaged over this C_l range to improve data quality.

In Table 2 the values for ΔC_d and $\Delta C_{l_{max}}$ corresponding to Figs. 9 and 10 are given. Also in Table 2 are the values for the case where the frost simulation extends from $x/c = 0.20$ to 0.60. Note that the baseline for these data is the clean model with the trip at $x/c = 0.20$ on the lower surface. With the roughness starting at the 20% location, the stagnation point does not move back on the roughness at high lift coefficients. Only the large frost and typical frost were tested, but in both cases the drag coefficient is reduced slightly by the presence of the roughness. While the effect is small, it was repeatable. The effect on maximum lift is less than the repeatability and not significant. The authors interpret that airfoil drag may have decreased via increased turbulence in the slot (due to the roughness) that may have caused a more efficient transition to turbulent flow on the flap. Hot-film measurements[18] have indicated laminar bubbles on the flap of this airfoil as shown in Fig. 3.

With the slat closed, the airfoil with simulated frost was studied for its Reynolds number dependence. Figure 11 shows the lift coefficient data for Reynolds numbers from 5×10^6 to 1.6×10^7 with the large frost simulation. No significant change in the lift curve slope is seen at the lower angles of attack, but α_{stall} and $C_{l_{max}}$ are affected. The $C_{l_{max}}$ increases with increasing Reynolds number as it did in the clean airfoil case of Fig. 5, although the magnitude is greater. The stall angle is reduced at Reynolds numbers 5×10^6 and 9×10^6, which was not seen in the clean data. Figure 12 shows the drag polars where the drag is seen to decrease with increasing Reynolds number. The magnitudes are similar to the clean case from Fig. 5.

The increments in maximum lift coefficient and drag coefficient are tabulated in Table 2 to show the Reynolds number effect. For the large frost case, shown in Figs. 11 and 12, a clear trend of decreasing $\Delta C_{l_{max}}$ with increasing Reynolds number is seen. The $\Delta C_{l_{max}}$ penalty due to the large frost of -0.073 at $Re = 5 \times 10^6$ decreases smoothly to an increase in $C_{l_{max}}$ at $Re = 16 \times 10^6$, where $\Delta C_{l_{max}} = 0.012$. The ΔC_d trend with Reynolds number is not as clear, but generally is increasing with increasing Reynolds number. The left two columns of Table 2 present the same data, but for the smaller roughness

Table 2 Change in C_d and $C_{l_{max}}$ slat-closed

	Trip x/c = 0.12 baseline, roughness 0.12 ≤ x/c ≤ 0.60					
	Typical frost		Large frost/ice		Large ice	
$Re \times 10^{-6}$	ΔC_d	$\Delta C_{l_{max}}$	ΔC_d	$\Delta C_{l_{max}}$	ΔC_d	$\Delta C_{l_{max}}$
5	——	——	0.00018	−0.073	——	——
9	0.00034	0.045	0.00035	−0.052	0.00095	0.016
12	0.00041	−0.006	0.00023	−0.035	——	——
16	0.00005	0.048	0.00040	0.012	——	——
	Trip x/c = 0.20 baseline, roughness 0.20 ≤ x/c ≤ 0.60					
9	−0.00037	0.0160	−0.00019	−0.012	——	——

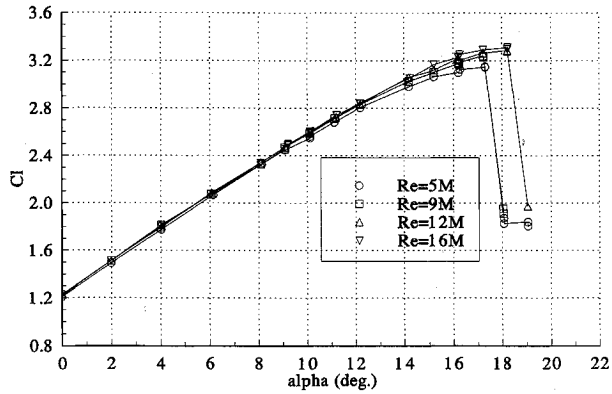

Fig. 11 Effect of Reynolds number on lift with large frost/ice, slat-closed, and roughness starting at x/c = 0.12.

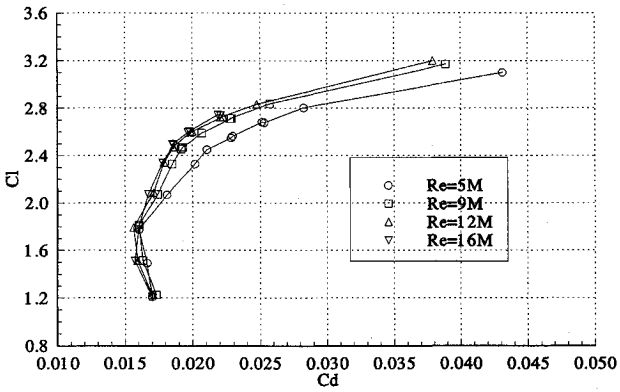

Fig. 12 Effect of Reynolds number on drag of the model with large frost/ice, slat-closed, and roughness starting at x/c = 0.12.

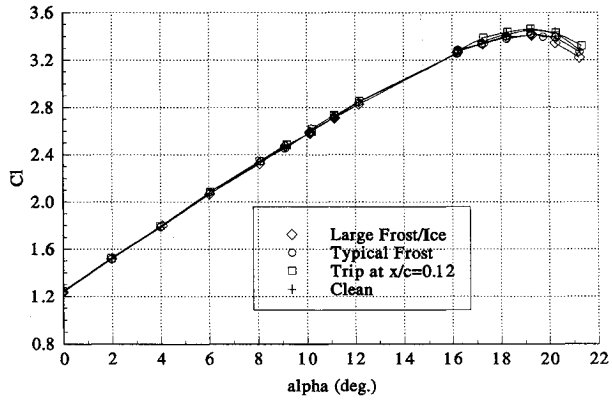

Fig. 13 Effect of simulated frost on lift at Re = 9 × 10⁶, slat-open, and roughness starting at x/c = 0.12.

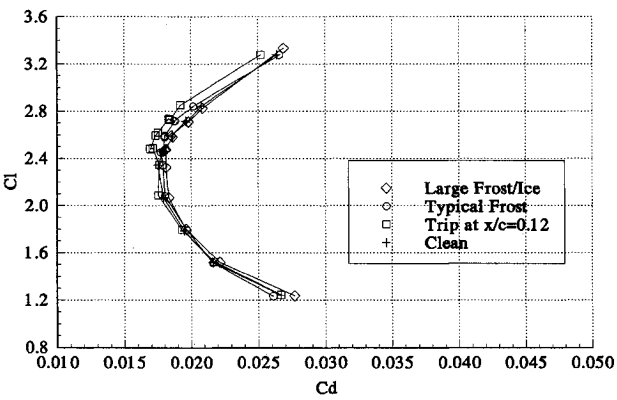

Fig. 14 Effect of simulated frost on drag at Re = 9 × 10⁶, slat-open, and roughness starting at x/c = 0.12.

size, typical frost simulation. Here, no discernible trends with Reynolds number are apparent, although the 5 × 10⁶ data are not available. While some trend in ΔC_d and $\Delta C_{l_{max}}$ with Reynolds number may actually be present, the magnitude of the effects are so close to the repeatability of the test that it cannot be deduced from this experiment.

Slat-Open with Simulated Frost

In analyzing the slat-open data, the likely presence of the laminar separation bubble must be taken into account. The bubble appears on the two-dimensional model unless the upper surface boundary-layer is tripped. On the actual swept wing the bubble may or may not appear, depending on the condition of the attachment line. For the discussion here, the clean baseline or the trip at x/c = 0.20 baseline will be used when the effect of frost on an airfoil with a bubble is desired, and the tripped baseline at x/c = 0.12 will be used when the effect of frost on an airfoil without a bubble is studied.

Figures 13 and 14 show the lift and drag coefficient data for two baselines and two frost simulations starting at x/c = 0.12 on the lower surface. The lift curve slope is not changed by the presence of the lower surface frost. In fact, the effect of the simulated frost is not seen in the lift data until beyond 16 deg angle of attack. The two frost simulations both suffer a decrease in $C_{l_{max}}$ of approximately 0.044 as compared to the clean and tripped baselines. The stall angles are the same. For this slat-open data the clean baseline will have the laminar bubble and the tripped baseline (at x/c = 0.12) will have eliminated the bubble, at least at the higher α. Therefore, the presence of the laminar bubble has little effect on the maximum lift or lift penalty in this case.

The effect on the drag coefficient is quite different. In the region of interest around V_2, C_l of 2.55–2.65, the minimum drag is seen when the boundary layer is tripped and the bubble is eliminated. The typical frost simulation has a drag value in the region of interest about halfway between the tripped and clean data. The typical frost trips the boundary layer eliminating the upper surface bubble, then increases the drag above the tripped value by further disturbing the upper surface

Table 3 Change in C_d and $C_{l_{max}}$ at $Re = 9 \times 10^6$, slat-open

	Roughness $0.12 \leq x/c \leq 0.60$					
	Trip $x/c = 0.12$ baseline			Trip $x/c = 0.20$ baseline		
	Typical frost	Large frost/ice	Large ice	Typical frost	Large frost/ice	Large ice
ΔC_d	0.00068	0.00129	0.00058	−0.00101	−0.00040	−0.00111
$\Delta C_{l_{max}}$	−0.043	−0.044	−0.146	−0.016	−0.017	−0.119
	Roughness $0.20 \leq x/c \leq 0.60$					
	Trip $x/c = 0.20$ baseline			Clean baseline		
	Typical frost	Large frost/ice	Large ice	Typical frost	Large frost/ice	Large ice
ΔC_d	−0.00042	−0.00039	—	0.00002	0.00005	—
$\Delta C_{l_{max}}$	−0.020	0.042	—	−0.039	0.023	—

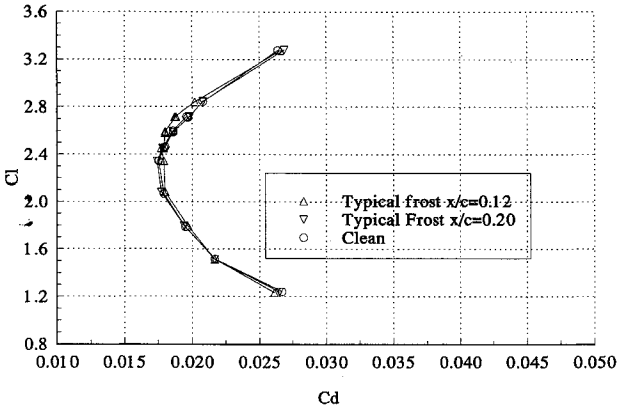

Fig. 15 Effect of frost starting location on drag at $Re = 9 \times 10^6$, slat-open.

boundary layer. The large frost also trips the boundary layer and creates even more drag by its larger disturbance of the boundary layer. In fact, it increases the drag by about the same amount as eliminating the bubble reduced the drag—thus making the clean airfoil and large frost simulation drag coefficients very similar. Table 3, roughness at $0.12 \leq x/c \leq 0.60$ and trip $x/c = 0.12$ baseline, shows that the large ice simulation has a drag penalty very similar to the typical frost. This does not seem to fit the pattern since the roughness size is so large. However, from Table I the roughness density for the large ice simulation is very low, which may explain this effect.

To consider the case of an airfoil with a leading-edge bubble, and frost starting at $x/c = 0.12$, refer to the data in Table 3 using the baseline of the airfoil tripped at $x/c = 0.20$. This is far enough back on the lower surface that the upper surface boundary layer is not affected by the trip. In this case, the frost actually reduces the drag by eliminating or reducing the effect of the bubble. However, the effect of the large ice on the maximum lift is significant whether the baseline eliminates the bubble or not.

For the frost simulation starting at $x/c = 0.20$ the presence of the bubble in the baseline is not important. Contamination of the lower surface this far from the leading edge and behind the stagnation point at the high angles of attack and, therefore, has no significant effects on the upper surface flow. Figure 15 shows drag data for the typical frost simulation starting at $x/c = 0.12$, $x/c = 0.20$, and clean airfoil data. While the $x/c = 0.12$ data reduces the drag from the clean value as discussed earlier, the $x/c = 0.20$ frost simulation has virtually no effect on drag. The maximum lift coefficient for frost starting back at $x/c = 0.20$ is also essentially the same as the clean data. These increments are summarized in Table 3 for two different baselines. The drag coefficients are actually reduced by the frost compared to the tripped baseline. Maximum lift is decreased slightly by the presence of the typical frost simulation and increased slightly by the large frost simulation.

Conclusions

Underwing frost has its largest effect on airfoil performance when it exists far enough forward to affect the upper surface boundary layer. When the frost/ice simulation was far enough back from the leading edge to prevent the contamination of the upper-surface boundary layer, the effect on lift and drag was very small. For the airfoil used in this study with a flap deflection of 15.6 deg, frost starting at $x/c = 0.20$ on the lower surface had little effect on the airfoil performance. This will of course be dependent on the airfoil geometry and flap deflection.

For this airfoil when the frost on the lower surface started at $x/c = 0.12$, the upper surface boundary layer was adversely affected at high angles of attack. In this case the degradation of airfoil performance was more distinct with the slat-gap open. This airfoil experienced a laminar separation bubble on the main element leading edge with the slat-open at Reynolds number 9×10^6. When the frost/ice eliminated the bubble a drag reduction was measured. If a trip was used on the baseline case to eliminate the bubble, the frost/ice increased the drag by the largest amounts measured in this study. The effect on maximum lift was significant in this case, particularly for the large ice simulation.

The large ice case considered in this experiment is unrealistically conservative and should not be applied to an operational situation. Considering only then the two frost simulations, in almost all cases the effect of the frost on the lower surface is small and within the threshold of data repeatability and estimated significance to the aircraft takeoff. While the effect of upper wing frost on aircraft takeoff is known to be a severe safety hazard, these tests indicate that for this airfoil under takeoff conditions, the effect of underwing frost is very small.

Acknowledgments

The authors from the University of Illinois were supported by the Federal Aviation Administration under Contract DTA03-92-C-00013. The authors would like to thank Charles Masters and James Riley at the FAA Technical Center for their contributions to this research, particularly in the area of aircraft operations with frost. Steve Robinson of NASA Langley made NASA resources available in a timely manner and contributed significantly to the test planning and data analysis. Our thanks also to Chet Dominik of McDonnell Douglas and Steve Wells, formerly at the University of Illinois, for their assistance in conducting the test. The staff of the NASA Langley Low-Turbulence Pressure Tunnel is gratefully acknowledged for the professional manner in which they conducted the test.

References

[1]Ljungstroem, B. L. G., "Wind Tunnel Investigation of Simulated Hoar Frost on a 2 Dimensional Wing Section with and Without High

Lift Devices," The Aeronautical Research Institute of Sweden, FFA-Au-902, Sweden, April 1972.

[3]Bragg, M. B., and Gregorek, G. M., "Environmentally Induced Surface Roughness Effects on Laminar Flow Airfoils: Implications for Flight Safety," AIAA Paper 89-2049, July 1989.

[3]Brumby, R. E., "The Effect of Wing Ice Contamination on Essential Flight Characteristics," *Proceedings of the Conference on Effects of Adverse Weather on Aerodynamics* (Toulouse, France), 1991, pp. 2-1–2-4 (AGARD-CP-496).

[4]Valarezo, W. O., Lynch, F. T., and McGhee, R. J., "Aerodynamic Performance Effects Due to Small Leading-Edge Ice (Roughness) on Wings and Tails," *Journal of Aircraft*, Vol. 30, No. 6, 1993, pp. 807–812.

[5]Valarezo, W. O., "Effects of Surface Roughness on Aircraft Performance," *Proceedings of the Ohio Aerospace Institute's Aircraft Icing Short Course* (Brookpark, OH), Ohio Aerospace Institute, OH, 1992.

[6]Bragg, M. B., and Gregorek, G. M., "Performance Analyses for Aircraft Icing Conditions," AIAA Paper 84-0180, Jan. 1984.

[7]Kind, R. J., and Lawrysyn, M. A., "Effects of Frost on Wing Aerodynamics and Take-Off Performance," *Proceedings of the Conference on Effects of Adverse Weather on Aerodynamics* (Toulouse, France), 1991, pp. 8-1–8-11 (AGARD-CP-496).

[8]Dietenberger, M., "A Proposed Simple and Safe Aircraft Take-Off or Landing Procedure with Wing Roughness or Protuberances," AIAA Paper 83-0604, Jan. 1983.

[9]Van Hengst, J., and Boer, J. N., "The Effect of Hoar-Frosted Wings on the Fokker 50 Take-Off Characteristics," *Proceedings of the Conference on Effects of Adverse Weather on Aerodynamics* (France), 1991, pp. 13-1–13-9 (AGARD-CP-496).

[10]Brumby, R. E., "Wing Surface Roughness Cause and Effect," *D.C. Flight Approach*, McDonnell Douglas Aerospace, No. 32, Jan. 1979, pp. 2–7.

[11]Langston, P. A. S., "Hoar Frost on Aircraft Surfaces," BEA Engineering, British Airways, TN P/570, Heathrow Airport, England, UK, Nov. 1968.

[12]Thompson, J. K., "Frost on Parked Aircraft," Wright Air Development Center, WADC TN 57-197, 1957.

[13]Kind, R. J., and Lawrysyn, M. A., "Aerodynamic Characteristics of Hoar Frost Roughness," AIAA Paper 91-0686, Jan. 1991.

[14]Valarezo, W. O., Dominik, C. J., McGhee, R. J., Goodman, W. L., and Paschal, K. B., "Multielement Airfoil Optimization for Maximum Lift at High Reynolds Numbers," AIAA Paper 91-3332, Sept. 1991.

[15]Paschal, K. B., Goodman, W. L., McGhee, R. J., Walker, B., and Wilcox, P., "Evaluation of Tunnel Sidewall Boundary-Layer-Control Systems," AIAA Paper 91-3243, Sept. 1991.

[16]Yip, L. P., Vijgen, P. H. M. W., Hardin, J. D., and Van Dam, C. P., "Subsonic High-Lift Flight Research on the NASA Transport Systems Research Vehicle (TSRV)," AIAA Paper 92-4103, Aug. 1992.

[17]Hardy, B. C., "Experimental Investigation of Attachment-Line Transition in Low-Speed High-Lift Wind-Tunnel Testing," *Proceedings of the Symposium on Fluid Dynamics of Three-Dimensional Turbulent Shear Flows and Transition* (Cesme, Turkey), 1988, pp. 2-1–2-17 (AGARD-CP-438).

[18]Nakayama, A., Stack, J. P., Lin, J. C., and Valarezo, W. O., "Surface Hot-Film Technique for Measurements of Transition, Separation, and Reattachment Points, AIAA Paper 93-2918, July 1993.

[19]Braslow, A. L., and Knox, E. C., "Simplified Method for Determination of Critical Height of Distributed Roughness Particles for Boundary-Layer Transition at Mach Numbers from 0 to 5," NACA TN 4363, Sept. 1958.

[20]Rae, W. H., and Pope, A., *Low-Speed Wind Tunnel Testing*, Wiley, New York, 1984, pp. 344–362.

[21]Valarezo, W. O., Dominik, C. J., and McGhee, R. J., "Multielement Airfoil Performance Due to Reynolds and Mach Number Variations," *Journal of Aircraft*, Vol. 30, No. 5, 1993, pp. 689–694.